

Two-phase flow simulation of aeration on stepped spillway^{*}

CHENG Xiangju, LUO Lin^{**}, ZHAO Wenqian and LI Ran

(State Key Laboratory of Hydraulics on High Speed Flows, Sichuan University, Chengdu 610065, China)

Received October 17, 2003; revised November 28, 2003

Abstract Stepped spillways have existed as escape works for a very long time. It is found that water can trap a lot of air when passing through steps and then increasing oxygen content in water body, so stepped spillways can be used as a measure of re-aeration and to improve water quality of water body. However, there is no reliable theoretical method on quantitative calculation of re-aeration ability for the stepped spillways. By introducing an air-water two-phase flow model, this paper used $k-\epsilon$ turbulence model to calculate the characteristic variables of free-surface aeration on stepped spillway. The calculated results fit with the experimental results well. It supports that the numerical modeling method is reasonable and offers firm foundation on calculating re-aeration ability of stepped spillways. The simulation approach can provide a possible optimization tool for designing stepped spillways of more efficient aeration capability.

Keywords: stepped spillway, two-phase flow, turbulence modeling, numerical simulation, water re-aeration.

Stepped spillways have been used for over 3500 years. During the 19th century, they were popular in Europe, North-America and Australia^[1]. The primary function of stepped spillways was limited to energy dissipation. Ruff^[2] and Chanson^[3] realized that stepped spillways have the intensive aeration ability after a series of detailed experimental investigations. Tozzi^[4], Chamani^[5], Boes^[6] and Cheng^[7] et al. have done a lot of experiments on free-surface aeration of stepped spillways one after another. All of these experiments, under different setups and flow conditions, cost a lot of money, resources and are very time consuming. This paper attempts to use a numerical simulation to solve this problem so as to save time, manpower and material resources.

Comparing the results from numerical simulation and experimental results from Chanson^[8], the calculated results fit with the experimental results well.

1 Numerical simulation approach

1.1 Governing equations

Volume of Fluid (VOF) model is applicable to the interface tracking between two or multi phases that are not interpenetrated. For each phase, a variable is introduced: the volume fraction of the phase in the computational cell, by which the interface between phases can be determined.

If the q th fluid's volume fraction in the cell is denoted as α_q , three possible situations are:

$\alpha_q = 0$: the cell is empty of the q th fluid,

$\alpha_q = 1$: the cell is full of the q th fluid, and

$0 < \alpha_q < 1$: the cell contains the interface between the q th fluid and one or more other fluid(s).

The sum of volume fraction of all phases in the computational cell is equal to 1,

$$\sum_{q=1}^n \alpha_q = 1. \quad (1)$$

(i) Continuity equation

Except the primary phase, the continuity equation to solve the volume fraction of the other phase(s) is

$$\frac{\partial \alpha_q}{\partial t} + u_i \frac{\partial \alpha_q}{\partial x_i} = 0, \quad (2)$$

and the volume fraction of the primary phase is determined by Eq. (1).

(ii) Momentum equation

$$\frac{\partial \rho u_i}{\partial t} + \frac{\partial}{\partial x_i} (\rho u_i u_j) = - \frac{\partial P}{\partial x_i} + \frac{\partial}{\partial x_j} \left[(\mu + \mu_t) \left(\frac{\partial u_i}{\partial x_j} + \frac{\partial u_j}{\partial x_i} \right) \right], \quad (3)$$

in which μ is the molecular viscosity, μ_t is the turbu-

^{*} Supported by the National Natural Science Foundation of China (Grant No. 50079013)

^{**} To whom correspondence should be addressed. E-mail: luolin@tsinghua.org.cn

lence viscosity, determined by the turbulent kinetic energy k and turbulence dissipation rate ϵ

$$\mu_t = \rho C_\mu \frac{k^2}{\epsilon}$$

(iii) Turbulence kinetic energy k equation

$$\frac{\partial(\rho k)}{\partial t} + \frac{\partial(\rho u_i k)}{\partial x_i} = \frac{\partial}{\partial x_i} \left[\left(\mu + \frac{\mu_t}{\sigma_k} \right) \frac{\partial k}{\partial x_i} \right] + G - \rho \epsilon, \quad (4)$$

in which G is production term of the turbulence

$$G = \mu_t \left(\frac{\partial u_i}{\partial x_j} + \frac{\partial u_j}{\partial x_i} \right) \frac{\partial u_i}{\partial x_j} \quad (5)$$

(iv) Turbulence kinetic dissipation rate ϵ equation

$$\frac{\partial(\rho \epsilon)}{\partial t} + \frac{\partial(\rho u_i \epsilon)}{\partial x_i} = \frac{\partial}{\partial x_i} \left[\left(\mu + \frac{\mu_t}{\sigma_\epsilon} \right) \frac{\partial \epsilon}{\partial x_i} \right] + C_{1\epsilon} \frac{\epsilon}{k} G - C_{2\epsilon} \rho \frac{\epsilon^2}{k} \quad (6)$$

The parameters in the above equations, such as density, viscosity, are calculated by weighted average method. For example, $\rho = \sum_{q=1}^n \alpha_q \rho_q$.

In the above equation system, C_μ , σ_k , σ_ϵ , $C_{1\epsilon}$, $C_{2\epsilon}$ are empirical constants and the standard model values are adopted (see Table 1).

Table 1. Values of empirical constant

C_μ	$C_{1\epsilon}$	$C_{2\epsilon}$	σ_k	σ_ϵ
0.09	1.44	1.92	1.0	1.3

Eqs. (1) ~ (6) consist of the closure system to solve the air-water two-phase flow problem in this project.

1.2 Boundary conditions

The computation setup after Chanson's experiment is adopted. 2D domain is used in the computation. The boundary conditions are shown in Fig. 1.

1.2.1 Inflow boundary The water inflow boundary is set as velocity-inlet condition. From the experiment case of Chanson, the inflow velocity is equal to 0.12127 m/s. The turbulence kinetic energy k and the turbulence dissipation rate ϵ of the inflow are calculated from the empirical equations as follows:

$$k = 0.00375 U_{in}^2, \quad (7)$$

$$\epsilon = k^{1.5} / (0.4 H_0), \quad (8)$$

in which H_0 is the water depth of the inflow.

The gas inflow is set as pressure-inlet condition.

The atmospheric pressure is used.

1.2.2 Outflow boundary The free flow condition is adopted in the case. The water depth of the outflow is flexible, and the water could not be separated from the air, so the pressure outflow condition is adopted. The normal gradients of all the variables are set to 0, $\frac{\partial \phi}{\partial n} = 0$, ϕ represents u , v , k , and ϵ , respectively.

1.2.3 Wall boundary The wall is set as the stationary wall of non-slip, i.e. $u = 0$ and $v = 0$. The viscosity layer near to the wall is treated with the wall function.

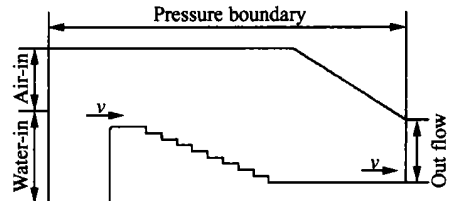


Fig. 1. Boundary conditions of calculation domain.

1.3 Numerical method

The finite volume method is adopted to solve the equations. The unstructured mesh is implemented to fit the complex domain shape. The pressure-implicit with splitting of operators (PISO) is applied to solving pressure-velocity coupling equations. The PISO approach is highly recommended for all transient flow calculations.

2 Experimental apparatus

The experimental apparatus and the experimental results are cited from Ref. [8]. Water is supplied from a large feeding basin leading to a sidewall with 4.8:1 contraction ratio. The test section consisted of a broad-crested weir (1-m wide, 0.6-long, with upstream rounded corner (0.057-m radius)) followed by nine identical steps ($h = 0.1$ m, $l = 0.25$ m) made of marine ply (Fig. 2). Steps are orderly numbered 1, 2, ... from top to toe of the weir. The characteristic variables of water-air fluid on steps when discharge Q is equal to 0.182 m³/s are shown in Fig. 5 to Fig. 11. C is the ratio of the volume of air bubbles in an air-water mixture of unit volume, y is the distance (m) from the pseudo-bottom (formed by the step edges) measured perpendicular to the measuring point, Y_{90} is the y (m) where the air concentration is 90%, V is velocity (m/s), V_{90} is charac-

teristic velocity (m/s) where the air concentration is 90%.

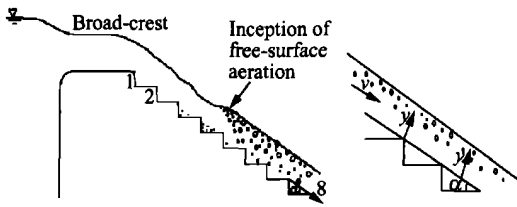


Fig. 2. Definition sketch of the test section.

3 Comparison between calculation results and experimental results

The shape and size of calculation domain is the same as the experimental apparatus used in Ref. [8]. Fig. 3 shows the velocity vectors from the top to the toe of the weir. It is found that there are obvious clockwise vortices in every step. These vortices can trap air into water, and meanwhile, some water droplets jump onto water surface, then exchange of water and air will happen. In order to visualize the distribution of turbulence kinetic energy on stepped spillway, Fig. 4 displays the contours of turbulence kinetic energy on step 6, step 7 and step 8. It can be seen that the turbulence kinetic energy on these steps has a maximum core within the step, and decreases rapidly in the radiation direction. In turbulent water flows, air bubbles may be entrained when the turbulence kinetic energy is large enough to overcome both

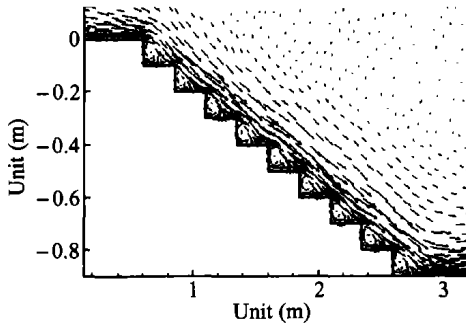


Fig. 3. Velocity vectors on stepped spillway.

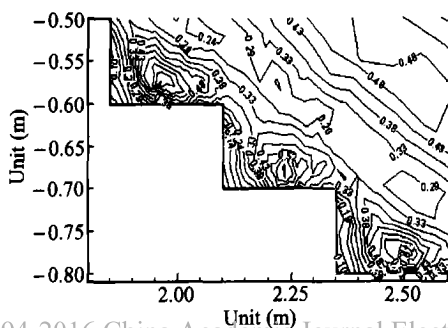


Fig. 4. Contours of k on steps 6, 7, 8.

surface tension and gravity effects. The k profiles can provide a clear image for air-laden water flow on the stepped spillway, then. The relations of void fraction C with y/Y_{90} on step 6, step 7 and step 8 are displayed in Fig. 5 to Fig. 8. The relations of V/V_{90} with y/Y_{90} of step 6, step 7 and step 8 are displayed in Fig. 9 to Fig. 11.

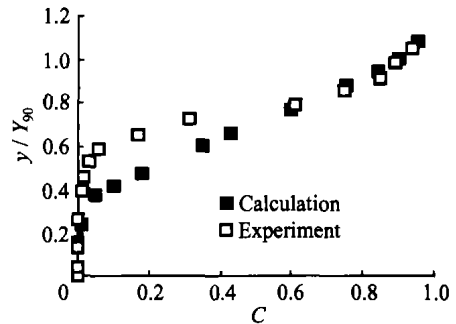


Fig. 5. Relation of C and y/Y_{90} on step 6.

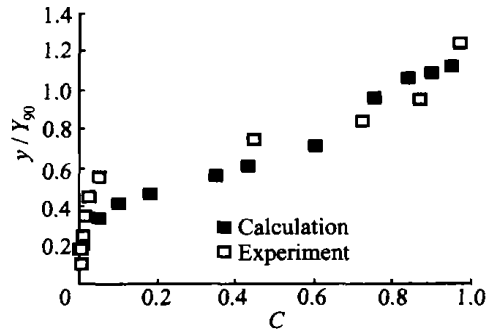


Fig. 6. Relation of C and y/Y_{90} on step 7.

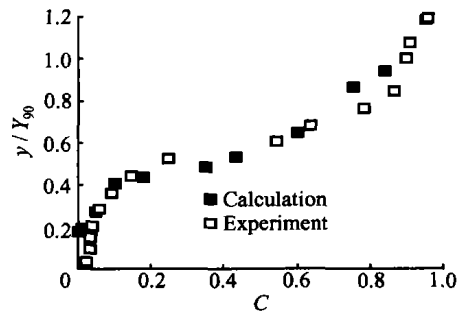


Fig. 7. Relation of C and y/Y_{90} on step 8.

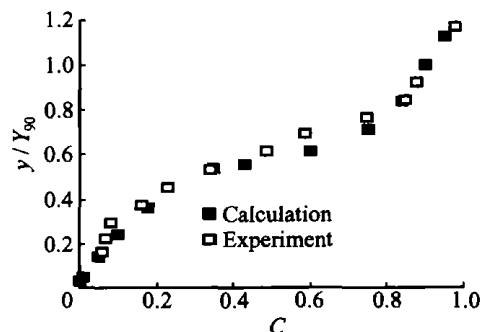


Fig. 8. Relation of C and y/Y_{90} between step 7 and step 8.

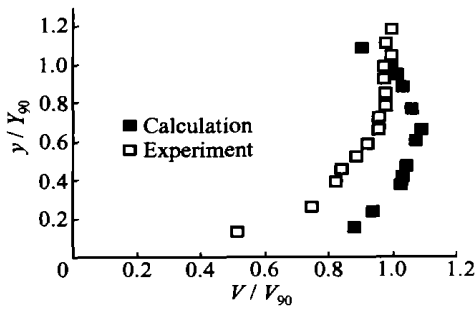


Fig. 9. Relation of V/V_{90} and y/Y_{90} on step 6.

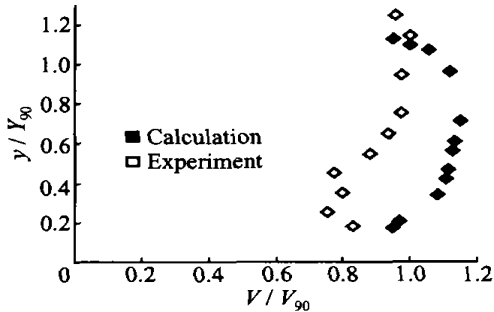


Fig. 10. Relation of V/V_{90} and y/Y_{90} on step 7.

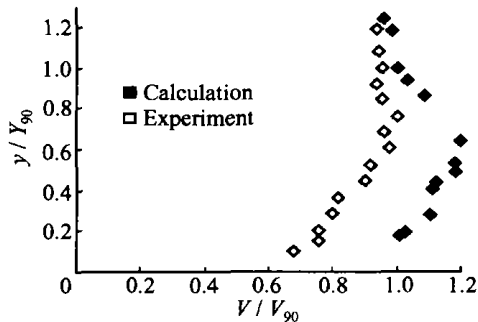


Fig. 11. Relation of V/V_{90} and y/Y_{90} on step 8.

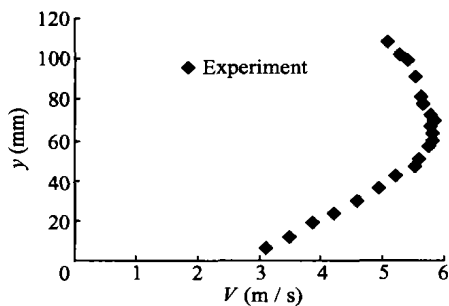


Fig. 12. Relation of V and y (from [5]).

From the relations between void fraction C and y/Y_{90} (see Figs. 5 ~ 8), the calculated results agree well with the experimental results. The void fraction C increases with y . It is because the contact area between the air and the water is small near the step edges the interaction of the air and the water is

weak, so it is difficult for air bubbles to be entrained into the water. When the distance y is increasing, the contact area between air and water is increasing correspondingly, so the void fraction C is increasing. Compared the relations between V/V_{90} and y/Y_{90} on step 6, step 7 and step 8, it is found that the calculated results have deviation from the experimental results. The values of V/V_{90} gotten from experiment are less than 1, say, the maximum velocity is at the place where the C is equal to 0.9. However, the velocity increased with the y until reaching a maximum value and then decreased as y increased further from the calculation data, and the maximum value of velocity is not at the place of Y_{90} . The places of the maximum values range from $C=0.4$ to 0.7 .

Chamani^[5] did some detailed experiments on the relation of the velocity and the normal distance y from the pseudo-bottom (see Fig. 12). Chamani thought that the air-water mixture velocity increased continuously with y until reaching a maximum value at a distance of y_{um} , and found that the y_{um} was generally smaller than Y_{90} . The value of C varies from 0.4 to 0.7 corresponding to the y_{um} . Compared the calculated results in this paper and the experimental results that Chamani got, it is found that both are very similar.

The authors think that the difference between the calculated and the Chanson's results, or between the Chamani's and the Chanson's results, came from the difference of measurement approaches. The Chanson's measurement equipment may probe the air-water mixture a different way for air-water two-phase flow with the Chamani's.

4 Conclusions

By introducing air-water two-phase flow methodology, this paper uses the $k-\epsilon$ turbulence model to calculate the characteristic variables of free-surface aeration on a stepped spillway. The calculated results fit with the experimental results well. The numerical simulation solved the problem of characteristic variables of self-aeration on stepped spillways theoretically, and it may save time and money for experimental researches. The approach described here can easily be used as a guideline of a real engineering, in which a lot of work needs to be done before the indoor experiment results can be used, for the scale effect. It can provide firm foundation for calculation of dissolved oxygen ability on stepped spillways as well.

The latter should be suitable for optimum design of a high efficient dissolved oxygen enhancement structure in a river, which is the target of the authors for pursuing.

References

- 1 Chanson, H. Forum article hydraulics of stepped spillways: current status. *J. Hyd. Engrg., ASCE*, 2000, 126(9): 636.
- 2 Ruff, J. F. et al. Air concentration measurements in highly-turbulent flow on a steeply-sloping chute. *Proc. Hydraulic Engineering Conf., ASCE, Buffalo USA, 1994*, 2: 999.
- 3 Chanson, H. Stepped spillway flows and air entrainment. *Can. J. Civil Eng.*, 1993, 20(3): 422.
- 4 Tozzi, M. et al. Air concentration in flows over stepped spillways. *Pro. 1998 ASME Fluids Eng. Conf., FEDSM' 98, Washington DC, 1998*, 6.
- 5 Chamani M. R. et al. Characteristics of skimming flow over stepped spillways. *J. Hyd. Engrg., ASCE*, 1999, 125(4): 361.
- 6 Boes, R. M. Physical model study on two-phase cascade flow. In: *Proc. 28th IAHR Congress (CD-ROM), Graz, Austria, 1999*.
- 7 Cheng, X. J. et al. Experimental study on re-aeration of artificial roughed spillway dams. *Water Resources and Hydropower Engineering (in Chinese)*, 2003, 34(9): 44.
- 8 Chanson H. Experimental investigations of air entrainment in transition and skimming flows down a stepped chute. *Can. J. Civ. Eng.*, 2002, 29: 145.